JOURNAL OF AIRCRAFT
Vol. 45, No. 4, July–August 2008

Aircraft Wake Vortex Measurement with Airborne Coherent Doppler Lidar

Stephan Rahm* and Igor Smalikho*
DLR, German Aerospace Center,
82234 Wessling, Germany

DOI: 10.2514/1.32896

An experiment for airborne Doppler lidar measurement of wake vortices generated by a large transport aircraft in the free atmosphere has been successfully carried out. In this paper, the description of the experiment, data processing procedure, and measurement results are given. It was shown that the use of smoke generators placed on large transport aircraft wings allows some high-quality wake vortex measurements with 2 μm coherent Doppler lidar installed in a second aircraft.

Introduction

THE investigation of aircraft wake vortices is important at present for the safety of air traffic. Coherent Doppler lidar (CDL) is a powerful technique for detection and study of aircraft wakes. Wake vortices generated by an aircraft flying in the atmospheric boundary layer can be measured with CDL in a ground-based configuration [1–9]. In the case of aircraft flight in the free atmosphere, the wake vortex measurement is practically possible only with airborne CDL placed in another aircraft. The results of wake vortex measurements with 2 μm CDL in an airborne configuration are published in [10], where, for vortex generation, a small aircraft (ATTAS, Advanced Technologies Testing Aircraft System) operated by DLR Braunschweig was used. The lidar system was installed in the Falcon aircraft and the experiment was carried out in April 2005. In November 2006, a similar experiment was conducted, where we measured wake vortices generated by a large transport aircraft (LTA). To provide strong lidar signals (SNR ≥ 1, where SNR is the ratio of mean signal power to the mean noise power within the bandwidth of 50 MHz) we used smoke generators. In contrast with ATTAS measurements, in this experiment, two smoke generators were used to seed both the port and the starboard vortices.

This paper describes the experiment on the measurement of wake vortices generated by the LTA as well as the procedure of data processing. In this procedure, the effect of the smoke seeding on measured lidar signals is taken into account. Data of the Falcon and LTA flights during these experiments (coordinates, aircraft speed) allowed us to estimate the age of each vortex measured by the lidar. After processing of the lidar data, the results for the wake vortex characteristics as a function of the vortex age were obtained. The paper presents these results.

Experiment

For measurement of wake vortices generated by an LTA, the airborne 2 μm Doppler lidar integrated in the DLR research aircraft Falcon F20 was used. In [10], the main parameters of the lidar and the integration of transceiver and scanner units in the Falcon are described.

The experiment was carried out on 9 and 15 November 2006 in a region between Toulouse and the Pyrenees in southern France. The measurements were conducted with clear weather and a northern wind (first day) and a southern wind (second day). The Falcon and LTA flight path and the laser beam scanning were used similar to in the previous experiment with ATTAS aircraft [10]. There was one flight (flight N1) on the first day and three flights (flights N2, N3, N4) on another day of the experiment. During each flight, the aircraft flew in the opposite direction to each other at the selected region (see Fig. 4 in [10], where instead of ATTAS aircraft should be an LTA). The altitude of the LTA flight was approximately 2700 m (flights N1 and N2) and 3600 m (flights N3 and N4). The Falcon operated about 900 m higher than the LTA. During flight N1 and flight N2, the speed (true aircraft speed, TAS) of the LTA was 90 m/s and the speed of the Falcon was 115 m/s. For flights N3 and N4, the TAS was 95 m/s (LTA) and 125 m/s (Falcon). Table 1 shows time periods (UTC, universal time coordinated) of flights of the Falcon and LTA. Each flight contained eight legs, that is, eight times the Falcon passed a point over the LTA and then the lidar could measure the wake vortices during each laser beam scan. After each turn, approximately 140 s before passing this point, the smoke generators installed below the wings of the LTA were switched on, and when Falcon has passed over the LTA, the smoke was switched off. The smoke OFF time (UTC) is given in Table 2. The interval between moments of the smoke switching off was from 7 up to 20 min (in mean for all flights and legs, 9 min). The pilot of the Falcon adjusted its flight direction to follow the smoke-seeded wake (sometimes transferred by crosswind) to keep the smoke-seeded wake within the laser beam scanning area. Maximum and minimum scan (nadir) angle was +15 and −15 deg, respectively. Scan rate was 10 deg/s, that is, 3 s for one scan.

Trajectories of all flights of the aircraft [global positioning system (GPS) data] are shown in Fig. 1. In the case of flights N1, N3, and N4, the lidar measurements of wake vortices were carried out when the aircraft were flying approximately along a north–south direction. During flight N2, the wake vortices were measured, when the aircraft were flying along an east–west direction.

Figure 2 shows an example of flight trajectories of the Falcon and the LTA in horizontal plane (X, Y) in a coordinate system with origin at lat = 0.834086 deg and long. = 43.075592 deg, or at initial position of the Falcon at UTC = 12:20:00 (see Table 1, flight N3). Corresponding parts of the LTA trajectory (when the smoke was generated) and the Falcon trajectory (when the lidar measured the smoke-seeded wake vortices) do not coincide, except small areas around points of the switching off of the smoke generators. This is due to the southern crosswind, which transported the smoke-seeded wake, and the pilot of the Falcon followed this trail.

After the experiment, the measured lidar data (UTC, scan (or nadir) angle, monitor, and backscatter signals for each shot) and aircraft (Falcon and LTA) flight data (GPS latitude, longitude, altitude, roll and pitch angles, and true aircraft speed) were used for analysis of the wake vortices generated by the LTA.

Received 18 June 2007; revision received 10 January 2008; accepted for publication 11 January 2008.

*Research Scientist, Lidar Group, Institute of Atmospheric Physics, Oberpfaffenhofen.

Data Processing

The data processing includes three main steps: the estimation of 1) Doppler spectra, 2) vortex core position, and 3) vortex circulation.

Doppler Spectra

Figure 3 shows an example of lidar data measured at the ith shot. The first part is the monitor signal and the second part is the backscatter signal. From the monitor signal, one can estimate the intermediate frequency $f_{\mathrm{LO}}^{(i)}$ (for control of the frequency corresponding to zero velocity in the measured spectra), the pulse emission time $t_0 = m_0 T_s$, where $T_s = 2$ ns is the sampling interval, and the pulse duration σ_p. The backscatter signal $J_B(mT_s, \varphi_i)$ sampled at scan angle φ_i can be considered as a function of the sample number m, or the time after pulse emission $t = (m - m_0)T_s$, or the range $R = ct/2$ (c is the light speed), which is the distance between the lidar and the sensing volume. The information about the speed of the aerosol particles in the sensing volume can be extracted from the Doppler spectrum (that is, from the power spectrum of the backscatter signal), using the Doppler equation $V = f\lambda/2$, where V is the velocity, f is the frequency, and $\lambda = 2.02$ μm is the wavelength.

To obtain the Doppler spectra at different ranges R_l, we select M samples of $J_B(mT_s, \varphi_i)$ around the corresponding sample number m and multiply each sample by the Gaussian window function

$$W(m'T_s) = \left(\frac{T_s}{\sqrt{\pi}\sigma_W}\right)^{1/2} \exp\left[-\frac{(m' - M/2)^2 T_s^2}{2\sigma_W^2}\right]$$

that is, we obtain

$$J_W(m'T_s, R_l, \varphi_i) = J_B\left(\left\{[R_l/(cT_s/2)] + m_0^{(i)} - M/2 + m'\right\}T_s, \varphi_i\right) \cdot W(m'T_s) \tag{1}$$

where $R_l = R_0 + \Delta R l$, $l = 0, 1, 2, \ldots, 60$, $M = 2048$. For processing of data measured in this experiment, the range separation ΔR of 12 m, minimum range R_0 of 740 m, and maximum range of 1460 m are optimal. The Gaussian window width σ_W is set equal to the pulse duration σ_p, and hence the range resolution (longitudinal size of the sensing volume) is $\sim$94 m. By using the fast Fourier transform technique, we estimate the Doppler spectra

$$\hat{S}_D(\Delta f k, R_l, \varphi_i) = \left|\sum_{m'=0}^{M-1} J_W(m'T_s, R_l, \varphi_i) \exp(-2\pi j k m'/M)\right|^2 \tag{2}$$

Table 1 Time periods (UTC) of flights of Falcon and LTA

Flight N	Date	Flight time period
1	09 Nov. 2006	13:54–15:24
2	15 Nov. 2006	08:54–10:00
3	15 Nov. 2006	12:20–13:20
4	15 Nov. 2006	15:36–16:30

where $k = 0, 1, 2, \ldots, M-1$, $\Delta f = (MT_s)^{-1} = 0.244$ MHz, $j = \sqrt{-1}$.

To reduce fluctuations of the spectrum estimates $\hat{S}_D$, the spectra are accumulated (averaged) to obtain

$$S_D(f_k, R_l, \varphi_n) = N_a^{-1} \sum_{i'}^{N_a} \hat{S}_D\left(\Delta f k - f_{\mathrm{LO}}^{(i)}, R_l, \varphi_i\right) \tag{3}$$

where also the intermediate frequency $f_{\mathrm{LO}}^{(i)}$ is taken into account; $i = (n-1)N_a + i'$, $n = 1, 2, 3, \ldots$. For accumulation, we use $N_a = 5$ shots. Taking into account that the scanning speed is 10 deg/s and the pulse repetition frequency is 500 Hz, at $N_a = 5$, the elevation angle resolution is $\sim$0.1 deg and therefore the transversal resolution is 1.7 m at range of 1 km. This resolution turned out to be sufficient to measure wake vortices generated by a large aircraft. As a result, we obtain the 3-D array $S_D(f_k, R_l, \varphi_n)$, where the frequency f_k can be replaced by the velocity $V_k = f_k\lambda/2$, and then we reduced the frequency (velocity) range to the band of $[-25, 25$ m/s].

Vortex Core Position

The next step is to estimate the vortex core coordinates from measured Doppler spectra, normalized by the mean noise spectral level. To find these characteristics, we use a fixed threshold for each spectrum (Thr = const at different R_l and φ_n, to avoid the impact of spectral noise, at $N_a = 5$, a threshold of 3.5 turned out to be optimal) and obtain the negative $V_-(R_l, \varphi_n)$ and positive $V_+(R_l, \varphi_n)$ velocity envelopes. Then we estimate the vortex core positions: $\{R_{C1}, \varphi_{C1}\}$ (right vortex) and $\{R_{C2}, \varphi_{C2}\}$ (left vortex) as the position exactly between the minimum velocity of the negative envelope and the maximum velocity of the positive envelope [9].

The information about the vortex core coordinates allows us to obtain from the 3-D array $S_D(f_k, R_l, \varphi_n)$ a 2-D array $S_D(f_k, R_{C1}, \varphi_n)$ $[S_D(f_k, R_{C2}, \varphi_n)]$ of the Doppler spectra for different scan angles at fixed distance from the lidar to the right (left) vortex core. Figure 4 shows an example of such spectra (flight N1, leg N1) for different scans. In the figure, the spectral intensity is shown in colors from white (minimum) to black (maximum). Because of the smoke seeding, the maximum intensity in the spectra occurs around the core intersections.

Vortex Circulation

Vortex core positions $\{R_{C1}, \varphi_{C1}\}$, $\{R_{C2}, \varphi_{C2}\}$ and spectra $S_D(f_k, R_{C1}, \varphi_n)$, $S_D(f_k, R_{C2}, \varphi_n)$ can be used for estimation of the vortex circulation. The velocity envelopes $V_-(R_{C1}, \varphi_n)$, $V_+(R_{C1}, \varphi_n)$, $V_-(R_{C2}, \varphi_n)$, and $V_+(R_{C2}, \varphi_n)$ obtained from these spectra at fixed threshold [Thr(φ) = const] are not acceptable for circulation estimation. The matter is that, in our case of the high and inhomogeneous SNR (due to the smoke seeding), these velocity envelopes obtained at Thr(φ) = const = 3.5 can strongly differ from the velocity of the wake vortex in the interval $[\varphi_1, \varphi_2]$, where the circulation is estimated. The velocity envelopes corresponding to the vortex velocity can be obtained only by using a floating threshold Thr(φ) $\neq$ const. This threshold, as a function of scan angle φ, is calculated by a special algorithm (see Appendix). The algorithm employs 1) a model for the Doppler spectrum $S_D^{(M)}(f, R, \varphi)$, 2) the

Table 2 Smoke OFF time (UTC)

Leg N	Smoke OFF time (flight N1)	Smoke OFF time (flight N2)	Smoke OFF time (flight N3)	Smoke OFF time (flight N4)
1	13:59:06	08:56:20	12:26:24	15:38:04
2	14:11:28	09:03:00	12:35:00	15:45:11
3	14:31:58	09:12:14	12:42:52	15:52:24
4	14:45:12	09:22:04	12:50:14	15:59:15
5	14:53:42	09:31:05	12:57:17	16:06:34
6	15:03:24	09:41:08	13:04:20	16:13:23
7	15:11:30	09:49:00	13:11:46	16:20:40
8	15:21:28	09:58:42	13:18:36	16:27:24

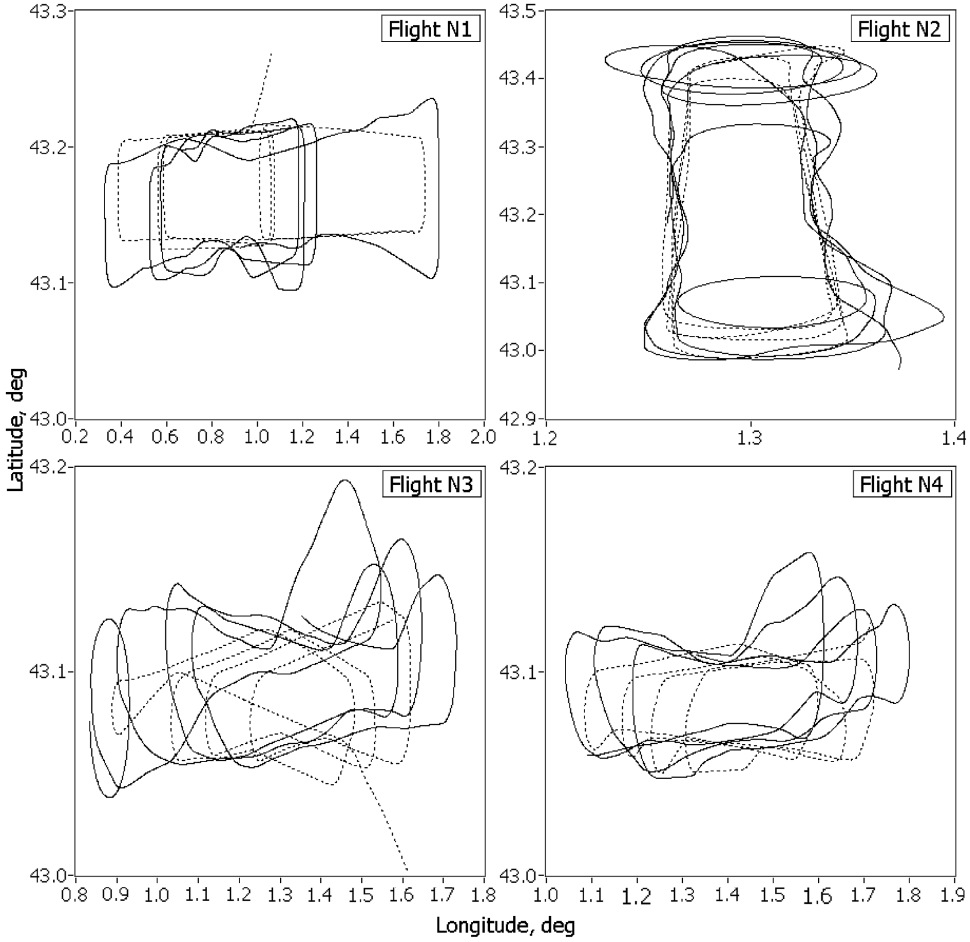

Fig. 1 Trajectories of Falcon (solid curves) and LTA (dashed curves) flights.

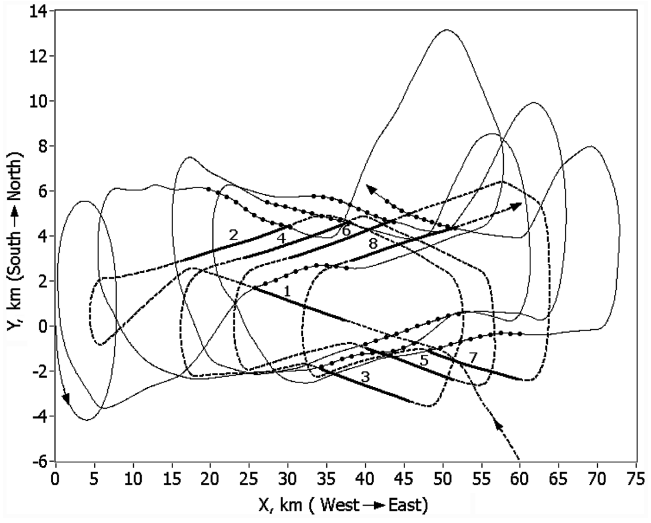

Fig. 2 Trajectories of Falcon (solid curve) flight and LTA (dashed curve) flight (flight N3). Heavy curves are areas with the smoke seeding (legs 1–8). Solid curves with dots shows areas where wake vortices were measured.

measured vortex core coordinates $\{R_{C1}, \varphi_{C1}\}$, $\{R_{C2}, \varphi_{C2}\}$, and 3) parameters of the signal-to-noise ratio SNR (see Appendix). Besides other parameters, the model $S_D^{(M)}(f, R, \varphi)$ also includes the vortex circulations (Γ_1 for right and Γ_2 for left vortex) which are unknown. Therefore, an iteration procedure is used. For the first iteration step, we assume a fixed threshold and from the obtained velocity envelopes, we estimate the circulations $\hat{\Gamma}_1$ and $\hat{\Gamma}_2$. With this intermediate result, we calculate in the second iteration step the floating threshold, and from the Doppler spectra we obtain new velocity envelopes. The vortex circulation is calculated by the integration method [11], using the integration interval from $R_{Cl}\varphi_1 =$ 5 m to $R_{Cl}\varphi_2 = 15$ m ($l = 1, 2$). Typically, two, maximum three, iterations with the floating threshold are sufficient to reach convergence.

Results

After the data processing, we have a set of 1) the vortex core position $\{R_{C1}(t_i), \varphi_{C1}(t_i)\}$, $\{R_{C2}(t_i), \varphi_{C2}(t_i)\}$ presented in a polar coordinate system related with Falcon (lidar) position, and 2) the vortex circulation $\hat{\Gamma}_1(t_i)$, $\hat{\Gamma}_2(t_i)$. They were measured at different time moments t_i (UTC), $i = 1, 2, 3, \ldots$. Using $\{R_{C1}(t_i), \varphi_{C1}(t_i)\}$, $\{R_{C2}(t_i), \varphi_{C2}(t_i)\}$ and data of Falcon and LTA flights (altitudes and horizontal coordinates of the aircraft, roll and pitch angles of the Falcon), we calculated core coordinates of the right $\{z_{C1}, \mathbf{r}_{C1}\}$ and the left $\{z_{C2}, \mathbf{r}_{C2}\}$ vortex, relative to the LTA position at time moment t_i, where z_{Cl} is vertical coordinate and $\mathbf{r}_{Cl} = \{y_{Cl}, x_{Cl}\}$ is the vector in the horizontal plane ($l = 1, 2$), axis X is directed along the trajectory of the LTA flight and axis Y is perpendicular to the flight direction (Y is directed from right to left side of the LTA). Vortex age τ_l was estimated by the equation $\tau_l = |\mathbf{r}_{Cl}|/V_a$, where V_a is the true speed of the LTA (meters per second).

Let us introduce the initial vortex core separation distance b (meters), the time t_0 (seconds) in which the vortex pair descends at the distance of one initial vortex core separation, and the theoretical root (initial) circulation Γ_0 (square meters per second). The parameters b, t_0, and Γ_0 are defined as [12]

$$b = (\pi/4)B_a \tag{4}$$

$$t_0 = 4\pi s^3\left(B_a^3/C_L V_a A\right) \tag{5}$$

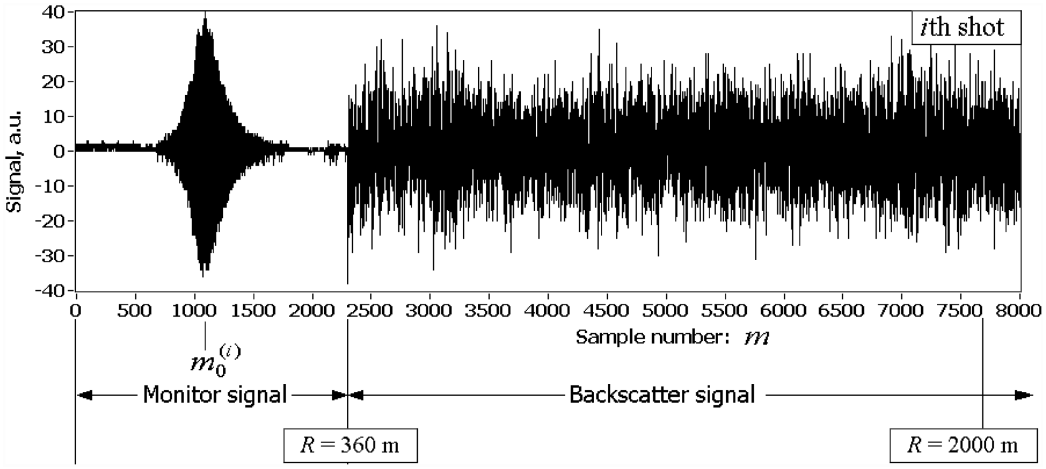

Fig. 3 Example of raw lidar data measured at the *i*th shot.

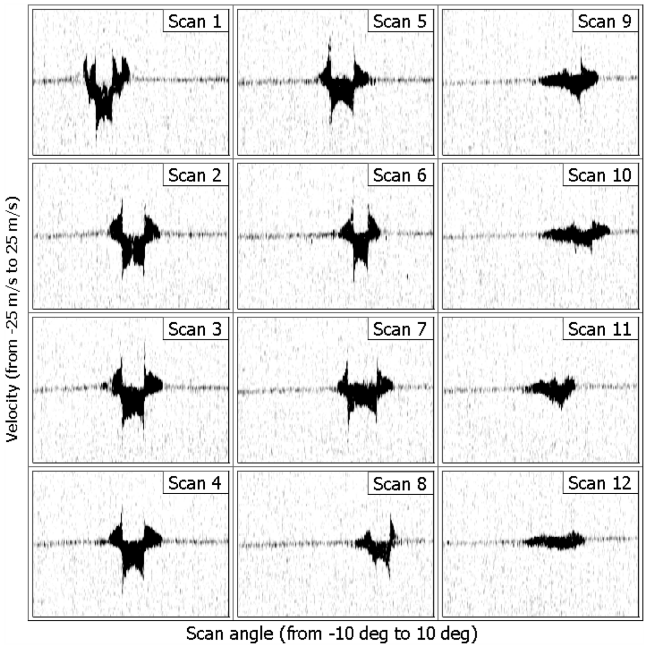

Fig. 4 Measured Doppler spectra (flight N1, leg N1).

$$\Gamma_0 = Mg/(s\rho B_a V_a) \tag{6}$$

where B_a is the wing span (meters), s is the spanwise load factor, C_L is the lift coefficient, A is the wing area (square meters), M is the aircraft mass (kilograms), g is the gravitational acceleration (meters per second squared), and ρ is the air density (kilogram per cubic meter). In this paper, we present the measurement results after normalization of the vortex characteristics: z_{Cl}/b, y_{Cl}/b, x_{Cl}/b, τ_l/t_0, and $\hat{\Gamma}_l/\Gamma_0$, where $l = 1, 2$.

Figure 5 shows an example for normalized horizontal coordinates of the wake vortices and normalized vertical coordinate (Fig. 5a) and circulation strength (Fig. 5b) vs normalized vortex age (Fig. 5c). These results were obtained from data measured at flight N1, leg N1. Because of the crosswind, the wake vortices were displaced along the Y axis with an increase of the distance ($|\mathbf{r}_{Cl}|$) between the vortex core and the LTA (see Fig. 5a). In this example, the displacement maximum $y_{Cl}/b \approx 10$ at $x_{Cl}/b \approx -400$. The wake vortices are in the field of each other and therefore, in undisturbed atmosphere, they have to sink only. The descent speed depends on the vortex circulation strength and the vortex core separation. In Fig. 5c, one can see that with an increase of the vortex age, after $\tau/t_0 \approx 2$, the rapid decay is observed and at $\tau/t_0 \approx 4.5$, the vortex circulation decreases by factor of two. Nevertheless, in Fig. 5b, we see almost linear dependence of vertical coordinates on the vortex age ($z/b \approx -\tau/t_0$) up to $\tau/t_0 \approx 5$. It can be explained by the effect of the vertical component of the background wind, that is, this component was directed downward at $\tau/t_0 > 2$.

Using the data measured in our experiment (4 flights or 32 legs), we obtained 768 estimates for each characteristic: z_{Cl}/b, y_{Cl}/b, x_{Cl}/b, τ_l/t_0, and $\hat{\Gamma}_l/\Gamma_0$. From these characteristics, one can estimate the vortex core separation $\hat{b} = |\{z_{C1}, \mathbf{r}_{C1}\} - \{z_{C2}, \mathbf{r}_{C2}\}|$. Averaging estimates of $\hat{b}$ obtained for $\tau/t_0 \le 1$ (73 estimates), we found that the mean value $<\hat{b}> \approx b$ and the standard deviation $\sigma_b = [<\hat{b}^2> - <\hat{b}>]^{1/2} \approx 0.14b$.

Figures 6 and 7 show vertical coordinates of the vortex core and vortex circulation, respectively, measured at different flights. Each curve corresponds to z_{Cl}/b ($\hat{\Gamma}_l/\Gamma_0$) vs vortex age τ_l/t_0 for right and left vortex, measured at one leg. For each flight, we have 16 such curves for z_{Cl}/b and $\hat{\Gamma}_l/\Gamma_0$. It is seen that the curves for z_{Cl}/b, measured at flight N1, are more smoothed, as compared with other flights. Flight N1 was on the first day, when a north–south wind took place, and flights N2–4 were on another day with a south–north wind. Probably, during our experiment on the second day, there was a large scale vertical wind structure in the atmosphere due to the southern wind over the Pyrenees (the experiment was carried out in a region between Toulouse and the Pyrenees). As a result, we measured strong variations of the vertical coordinate of the vortex core at flights N2–4.

All estimates (points) for the vertical coordinate of the vortex core and for the vortex circulation are shown in Figs. 8 and 9, respectively. In the experiment, the wake vortices were observed up to $\tau/t_0 \approx 8$. We selected the estimates in the interval $0 \le \tau/t_0 \le 5$ and calculated the mean value (solid curves in Figs. 8 and 9) of considered characteristics, using a moving window averaging procedure with a window width $\Delta\tau/t_0 = 1$. In Fig. 8, it is seen that the mean vortex descent ($<z/b>$, solid curve) is described by the linear equation $<z/b> = -\tau/t_0$ up to $\tau/t_0 \approx 3$. The scatter of the points around the solid curve (Fig. 8) is explained mainly by the effect of the vertical component of the wind on the wake vortices. For example, in the case of the lidar measurement during flight N3, leg N8 at $\tau/t_0 \le 2$, the vertical wind component V_Z was positive, that is, it was directed upward (estimate of V_Z can be obtained from our experimental data [9], that is, from measured radial velocity, taking into account the Falcon flight data) and $|V_Z|$ was larger than the vortex descent speed $V_d = b/t_0$. Therefore, in Fig. 8 for this case, we observe the exceeding of points over zero level. For the same flight (flight N3), but in the case of leg N3 and leg N7, the V_Z was negative (vertical wind direction is downward) and $|V_Z| > V_d$. Here, in interval $2 \le \tau/t_0 \le 3$, we observe a much stronger descent of the wake vortices, as compared with the mean descent. Besides measured lidar

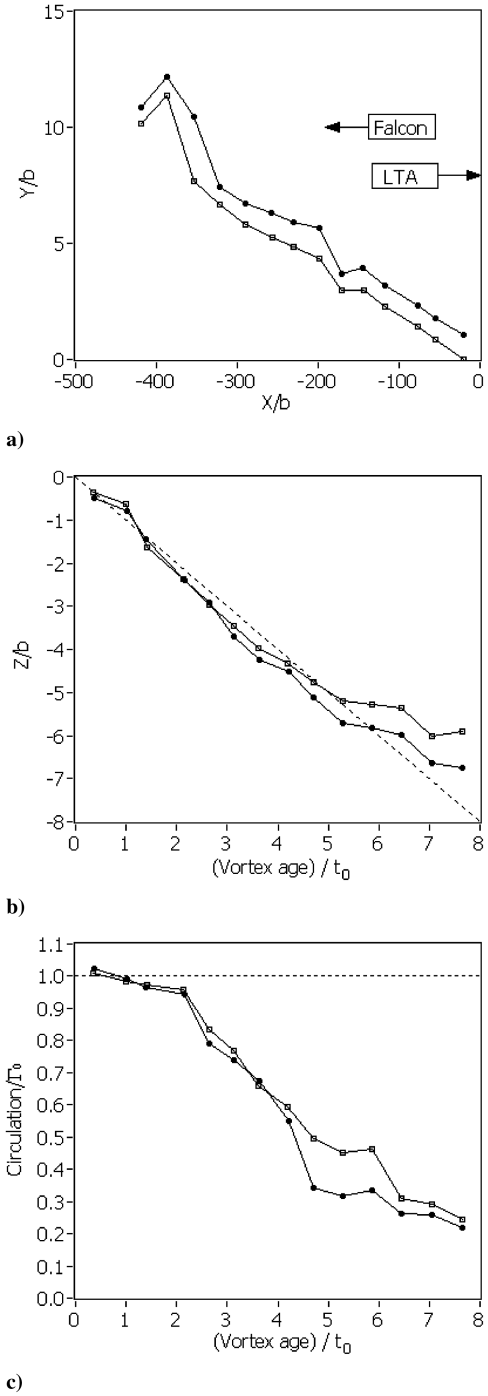

Fig. 5 Normalized horizontal coordinates a) of the wake vortices and normalized vertical coordinate, b) and circulation, c) vs normalized vortex age (flight N1, leg N1).

data (backscatter signal, scan angle) for estimation of $z_{Cl}(\tau)$, we used aircraft flight data of the Falcon and the LTA (UTC, latitude, longitude, altitude of the aircraft, pitch and roll angle of the Falcon). Errors in measurements of the aircraft flight data can also have an effect on the scatter of points in Fig. 8 and, therefore, a ground-based lidar measurement of the vortex descent $z_{Cl}(\tau)$ is more accurate than the airborne lidar measurement. For estimation of the vortex circulation, we used only the lidar data measured at very high SNR (due to the smoke seeding), and one can assume that the circulation estimates were obtained with high accuracy.

The solid curve shown in Fig. 9 can be split in two parts: 1) slow decay ($0 < \tau/t_0 < 3$), and 2) rapid decay ($\tau/t_0 > 3$). This result corresponds to the theoretical model of two-phase decay [13].

For the conditions of our experiment, we numerically simulated Doppler lidar signals (an algorithm of the simulation can be found, for example, in [14,15]), assuming a homogeneous atmosphere and using a Lamb–Oseen model for wake vortices. Then, for processing of the simulated data, we used the algorithm given in this paper and, from obtained results, we calculated the normalized standard deviations (errors) of the vertical coordinate of the vortex core $\sigma_{z/b}$ and the vortex circulation $\sigma_{\hat{\Gamma}/\Gamma_0}$. From the simulation data we have $\sigma_{z/b} = 0.13$ and $\sigma_{\hat{\Gamma}/\Gamma_0} = 0.033$. From experimental data (see Figs. 8 and 9), we calculated the standard deviations (scatter) of the estimates: 1.04 for the vortex descent and 0.085 for the vortex circulation. Because of the atmosphere (background wind, including turbulence and large scale variations) effect, the standard deviations from the experiment are essentially larger than correspondent measurement errors calculated from the simulated data.

Conclusions

The measurements of the wake vortices generated by an LTA in the free atmosphere (at an altitude of 2.7 km and 3.6 km in the region between Toulouse and the Pyrenees) were carried out with a 2 μm coherent Doppler lidar installed in the Falcon aircraft. The use of two smoke generators placed below the LTA wings allows the lidar measurements of the wake vortices independently from the background SNR (at any small concentration of atmospheric aerosol particles).

From all measured data, 768 estimates for each characteristic (horizontal trajectory, vertical coordinate, and circulation) of the wake vortex were obtained at different vortex ages. The statistical analysis of these estimates shows that, in mean, the vortex descent is described by the equation $\langle z/b \rangle = -\tau/t_0$ up to $\tau/t_0 \approx 3$, and the mean vortex circulation decay has two phases of the vortex evolution: a moderate decay up to $\tau/t_0 \approx 3$ that turns into a steeper slope characterizing the phase of rapid decay.

Errors of vortex characteristic measurement were estimated, using numerical simulation of the lidar data. These computed errors are much less than the corresponding scatter of experimental estimates from the mean value in Figs. 8 and 9. Therefore, the measurement accuracy in our experiment allows us to investigate the wake vortices generated by an LTA with the smoke generators in the free atmosphere under different atmospheric conditions.

Appendix: Calculation of Floating Threshold

The spectrum model $S_D^{(M)}(f, R, \varphi)$ is the mean (conditional averaged) Doppler spectrum. From the equation for the coherently detected backscatter signal $J_B(t, \varphi)$ [14,15] in the case of the Gaussian window $W(mT_s)$, the equation for the mean Doppler spectrum can be obtained using conditional ensemble averaging in the form

$$S_D^{(M)}(f, R, \varphi) = B \int_{-\infty}^{+\infty} \mathrm{d}z'\, Q_S(z') \times \frac{S_a(R + z', \varphi) + S_b}{\sqrt{2\pi}\sigma_{fP}} \exp\left\{ -\frac{[f - V_r(R + z', \varphi)2/\lambda]^2}{2\sigma_{fP}^2} \right\} + 1 \tag{A1}$$

where $f \in [-B/2, B/2]$ is the frequency, $B = 50$ MHz (50 m/s) is the spectral bandwidth, R is the range, φ is the scan angle, $Q_S(z') = \Delta z^{-1} \exp(-\pi z'^2/\Delta z^2)$ is the function of spatial resolution (averaging) along the laser beam axis z',

$$\Delta z = \sqrt{\pi}\sqrt{\sigma_p^2 + \sigma_W^2} \cdot c/2 \approx 94 \text{ m}$$

is the longitudinal size of the sensing volume, and

$$\sigma_{fP} = \frac{1}{2\pi\sqrt{2}} \frac{\sqrt{\sigma_p^2 + \sigma_W^2}}{\sigma_p \sigma_W} \approx 0.65 \text{ MHz} \quad (0.65 \text{ m/s})$$

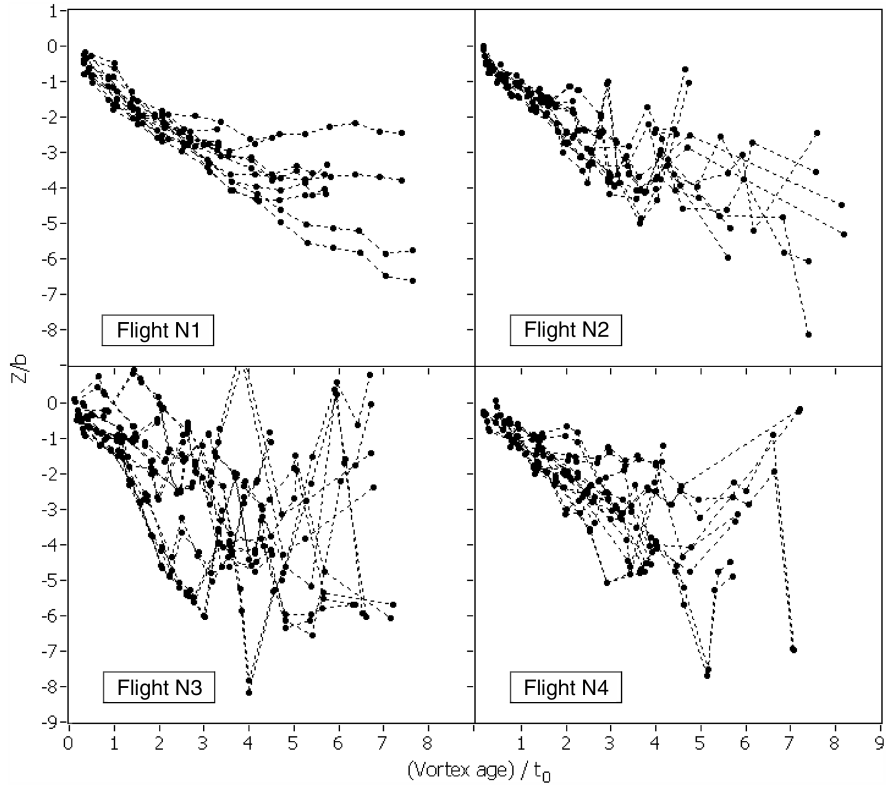

Fig. 6 Normalized vertical coordinate of the vortex core vs normalized vortex age, measured at different flights.

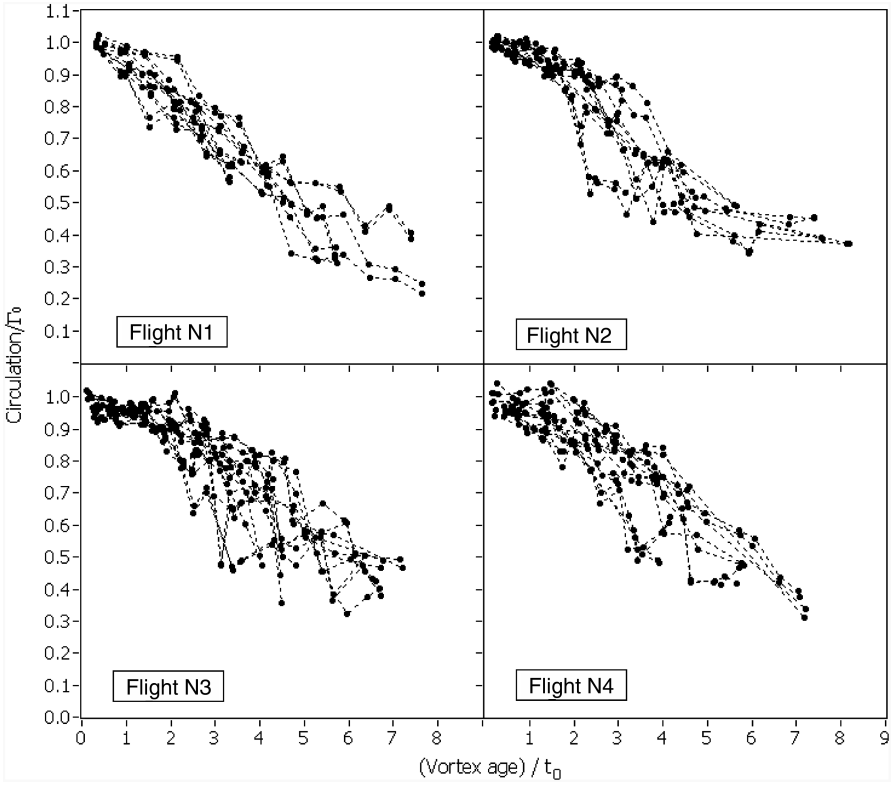

Fig. 7 Normalized vortex circulation vs normalized vortex age, measured at different flights.

is the Doppler spectrum width for the case of homogeneous radial velocity $[V_r(R) = \text{const}]$. The sum $S_a(R + z', \varphi) + S_b$ can be determined as normalized density of distribution of SNR along axis z' with contribution of the generated smoke $[S_a(R + z', \varphi)]$ and atmospheric aerosols S_b. In the case of the smoke-seeded wake, for calculation of the floating threshold, it is necessary to take into account dependence of SNR on R and φ. From (A1), we have the equation

$$\text{SNR}\,(R, \varphi) = B^{-1} \int_{-\infty}^{\infty} \left[S_D^{(M)}(f, R, \varphi) - 1 \right] \mathrm{d}f = S_b + \int_{-\infty}^{\infty} \mathrm{d}z' Q(z') S_a(R + z', \varphi) \tag{A2}$$

Without the smoke seeding, the SNR $= S_b$. We assume the Gaussian model for each plume (smoke-seeded wake), and for description of

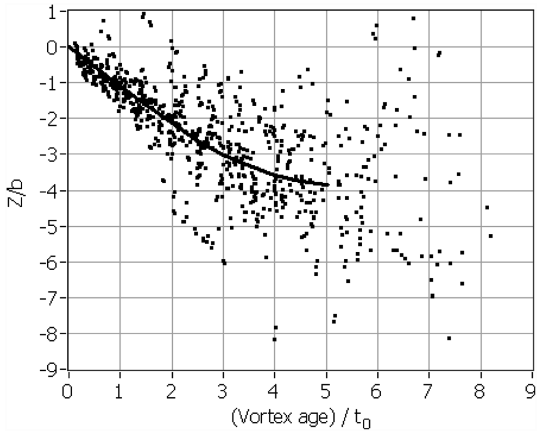

Fig. 8 Normalized vertical coordinate of the vortex core vs normalized vortex age.

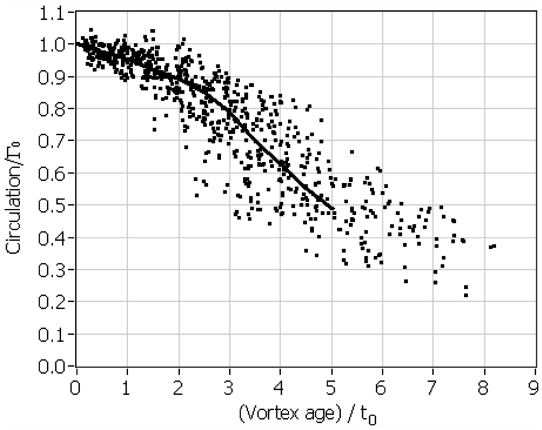

Fig. 9 Normalized vortex circulation vs normalized vortex age. Points are single estimates; solid curve is the mean value.

the plume pair, we use equation

$$S_a(R,\varphi) = \sum_{l=1}^{2} S_{ml} \exp\left\{-\frac{(R\cos\varphi - R_{Cl}\cos\varphi_{Cl})^2 + (R\sin\varphi - R_{Cl}\sin\varphi_{Cl})^2}{L_{sl}^2}\right\} \tag{A3}$$

where S_{ml} and L_{sl} are parameters of the model for the right ($l = 1$) and left ($l = 2$) plume. These parameters can be found by fitting the model described by Eqs. (A2) and (A3) to measured $\mathrm{SNR}(R_{Cl}, \varphi)$.

In Eq. (A1), we neglect the influence of turbulent variations of the wind and take into account only the effect of wake vortices on the radial velocity $V_r(R, \varphi)$. In the case of the ideal shape of the wake vortices, the radial velocity can be written as

$$V_r(R, \varphi) = \mathrm{Im}[\Phi V^{(2)}(R\Phi)] \tag{A4}$$

where $\Phi = \cos\varphi + j\sin\varphi$ is the vector directed along the laser beam (in complex form), $V^{(2)}(r) = V_1^{(1)}(r - r_1) - V_2^{(1)}(r - r_2)$ is the velocity vector of the vortex pair,

$$V_i^{(1)}(r) = \frac{\Gamma_i}{2\pi} \cdot \frac{\mu(|r|/r_C)}{r}$$

is the velocity vector of the lth single vortex in the coordinate system centered at the vortex core position r_i ($R_{Ci} = |r_i|$ is the distance from the lidar to the lth vortex core, $\varphi_{Ci} = -\arg[jr_i]$ is the scan angle at the core intersection), $r = y + jz$ is the radius vector, and r_C is the vortex core radius. For the Lamb–Oseen model, $\mu(x) = 1 - \exp(-1.256x^2)$.

If the wake vortex parameters Γ_i, R_{Ci}, φ_{Ci} (and r_C) and the "plume + lidar" parameters $S_b, S_{ml}, L_{sl}, \Delta z$, and σ_{fP} are known, one can calculate the radial velocity $V_r(R, \varphi)$ and the spectrum $S_D^{(M)}(f, R, \varphi)$ by Eqs. (A1–A4). For each vortex, we can also calculate the frequency

$$f_{\mathrm{thr}}^{(l)}(\varphi) = V_r(R_{Ci}, \varphi)2/\lambda \tag{A5}$$

corresponding to the radial velocity at a fixed distance from the lidar to the lth vortex core, as a function of the scan angle φ. Then, we calculate the spectrum model at frequency $f = f_{\mathrm{thr}}^{(l)}(\varphi)$. The spectrum model at such frequency is the floating threshold

$$\mathrm{thr}_l(\varphi) = S_D^{(M)}\left(f_{\mathrm{thr}}^{(l)}(\varphi), R_{Cl}, \varphi\right) \tag{A6}$$

which can be used for obtaining the velocity envelope from the measured spectrum. When $f_{\mathrm{thr}}^{(i)}(\varphi) < 0$ and $f_{\mathrm{thr}}^{(i)}(\varphi) > 0$, we obtain the negative and positive envelope, respectively.

Acknowledgment

The measurements were funded by the European Union AWIATOR program contract no. G4RD.CD200200836.

References

[1] Hannon, S. M., and Thomson, J. A., "Aircraft Wake Vortex Detection and Measurement with Pulsed Solid-State Coherent Laser Radar," *Journal of Modern Optics*, Vol. 41, No. 11, 1994, pp. 2175–2196. doi:10.1080/09500349414552031

[2] Köpp, F., "Doppler Lidar Investigation of Wake Vortex Transport Between Closely Spaced Parallel Runways," *AIAA Journal*, Vol. 32, No. 4, 1994, pp. 805–810.

[3] Constant, G., Foord, R., Forrester, P. A., and Vaughan, J. M., "Coherent Laser Radar and the Problem of Aircraft Wake Vortices," *Journal of Modern Optics*, Vol. 41, No. 11, 1994, pp. 2153–2173. doi:10.1080/09500349414552021

[4] Köpp, F., "Wake-Vortex Characteristics of Military-Type Aircraft Measured at Airport Oberpfaffenhofen Using the DLR Laser Doppler Anemometer," *Aerospace Science and Technology*, Vol. 3, No. 4, 1999, pp. 191–199. doi:10.1016/S1270-9638(99)80042-X

[5] Harris, M., Vaughan, J. M., Huenecke, K., and Huenecke, C., "Aircraft Wake Vortices: A Comparison of Wind-Tunnel Data with Field-Trial Measurements by Laser Radar," *Aerospace Science and Technology*, Vol. 4, No. 5, 2000, pp. 363–370. doi:10.1016/S1270-9638(00)00136-X

[6] Vaughan, J. M., and Harris, M., "Lidar Measurement of B747 Wakes: Observation of a Vortex Within a Vortex," *Aerospace Science and Technology*, Vol. 5, No. 6, 2001, pp. 409–411. doi:10.1016/S1270-9638(01)01115-4

[7] Harris, M., Young, R. I., Köpp, F., Dolfi, A., and Cariou, J.-P., "Wake Vortex Detection and Monitoring," *Aerospace Science and Technology*, Vol. 6, No. 5, 2002, pp. 325–331. doi:10.1016/S1270-9638(02)01171-9

[8] Köpp, F., Rahm, S., Smalikho, I., Dolfi, A., Cariou, J.-P., Harris, M., and Young, R. I., "Comparison of Wake-Vortex Parameters Measured by Pulsed and Continuous-Wave Lidars," *Journal of Aircraft*, Vol. 42, No. 4, 2005, pp. 916–923. doi:10.2514/1.8177

[9] Köpp, F., Rahm, S., and Smalikho, I., "Characterization of Aircraft Wake Vortices by 2-mm Pulsed Doppler Lidar," *Journal of Atmospheric and Oceanic Technology*, Vol. 21, No. 2, 2004, pp. 194–206. doi:10.1175/1520-0426(2004)021<0194:COAWVB>2.0.CO;2

[10] Rahm, S., Smalikho, I., and Köpp, F. "Characterization of Aircraft Wake Vortices by Airborne Coherent Doppler Lidar," *Journal of Aircraft*, Vol. 44, No. 3, 2007, pp. 799–805. doi:10.2514/1.24401

[11] Holzäpfel, F., Gerz, T., Köpp, F., Stumpf, E., Harris, M., Young, R. I., and Dolfi, A., "Strategies for Circulation Evaluation of Aircraft Wake Vortices Measured by Lidar," *Journal of Atmospheric and Oceanic Technology*, Vol. 20, No. 8, 2003, pp. 1183–1195. doi:10.1175/1520-0426(2003)020<1183:SFCEOA>2.0.CO;2

[12] Gerz, T., Holzäpfel, F., and Darracq, D., "Commercial Aircraft Wake Vortices," *Progress in Aerospace Sciences*, Vol. 38, No. 3, 2002, pp. 181–208. doi:10.1016/S0376-0421(02)00004-0

[13] Holzäpfel, F., Hofbauer, T., Darracq, D., Moet, H., Garnier, F., and Ferreira Gago, C., "Analysis of Wake Vortex Decay Mechanisms in the Atmosphere," *Aerospace Science and Technology*, Vol. 7, No. 4, 2003, pp. 263–275. doi:10.1016/S1270-9638(03)00026-9

[14] Salamitou, P., Dabas, A., and Flamant, P. H. "Simulation in the Time Domain for Heterodyne Coherent Laser Radar", *Applied Optics*, Vol. 34, No. 3, 1995, pp. 499–506.

[15] Banakh, V. A., and Smalikho, I. N. "Estimation of the Turbulence Energy Dissipation Rate from the Pulsed Doppler Lidar Data", *Atmospheric and Oceanic Optics*, Vol. 10, No. 12, 1997, pp. 957–965.